Stability, pharmacokinetics, and biodistribution in mice of the EPAC1 inhibitor (R)-CE3F4 entrapped in liposomes and lipid nanocapsules

Balthazar Toussaint, Hervé Hillaireau, Catherine Cailleau, Yves Ambroise, Elias Fattal

Stability, pharmacokinetics, and biodistribution in mice of the EPAC1 inhibitor (*R*)-CE3F4 entrapped in liposomes and lipid nanocapsules

Balthazar Toussaint[1,2], Hervé Hillaireau[1], Catherine Cailleau[1], Yves Ambroise[3], Elias Fattal[1,*].

[1] Université Paris-Saclay, CNRS, Institut Galien Paris Saclay, 92296, Châtenay-Malabry, France.

[2] Département de Recherche et Développement Pharmaceutique, Agence Générale des Équipements et Produits de Santé (AGEPS), Assistance Publique des Hôpitaux de Paris (AP-HP), Paris, France.

[3] Université Paris-Saclay, CEA, Institut des Sciences du Vivant Frederic-Joliot, 91191, Gif-sur-Yvette, France.

* Corresponding Author:
Elias Fattal, Ph.D
Université Paris-Saclay
Institut Galien Paris-Saclay
UMR CNRS 8612
5 Rue Jean-Baptiste Clément
92290 Châtenay-Malabry
France

Abstract

(*R*)-CE3F4, a specific inhibitor of EPAC1 (exchange protein directly activated by cAMP type 1), has been demonstrated *in vitro* and *in vivo* to reduce hypertrophic signaling contributing to heart failure or to control arrhythmia and has shown promise as a drug candidate. However, (*R*)-CE3F4 exhibits poor solubility in aqueous media and has shown sensitivity to enzyme hydrolysis in plasma. To overcome these issues, the drug was entrapped in liposomes and lipid nanocapsules. Both systems considerably increased the drug apparent solubility in aqueous media. Among these nanocarriers, lipid nanocapsules offered significant protection *in vitro* against enzymatic degradation by increasing the (*R*)-CE3F4 apparent half-life from around 40 min to 6 h. Pharmacokinetics and biodistribution of (*R*)-CE3F4 radiolabeled or not were studied in healthy C57BL/6 mice. The non-encapsulated ^{3}H-CE3F4 showed a very rapid distribution outside the blood compartment. Similar results were observed when using nanocarriers together with a fast dissociation of ^{3}H-CE3F4 from nanocapsules simultaneously labeled with ^{14}C. Thus, essential preclinical information on CE3F4 fate has been obtained, as well as the impact of its formulation using lipid-based nanocarriers.

Keywords:

EPAC1 inhibitors, liposomes, nanocapsules, stability, pharmacokinetics, biodistribution

1. ***Introduction***

Cardiovascular diseases are still the first causes of death according to World Health Organization and the number of death increased during the two last decades (World Health Organization, 2020) despite the improvement in the care and therapeutic armamentarium. This leads to the research of new interesting pharmacological targets and drug candidates to treat cardiac diseases.

Over the past two decades, the exchange protein directly activated by cAMP 1 (EPAC1) has been increasingly documented as a pharmacological target of various diseases. This protein is ubiquitously expressed and involved in numerous signaling pathways (Robichaux and Cheng, 2018). Its downregulation has shown promises to treat Alzheimer's disease (McPhee et al., 2005), breast, gastric, and pancreatic cancers (Kumar et al., 2017; Lorenz et al., 2008; Sun et al., 2017), heart failure (Metrich et al., 2010), arrhythmia (Hothi et al., 2008) and depression (Middeldorp et al., 2010).

(*R*)-CE3F4 (**Figure 1**) has been identified as a drug candidate to treat cardiac diseases because it is a specific and uncompetitive inhibitor of EPAC1 (Courilleau et al., 2013, 2012). Indeed, this tetrahydroquinoline analog has demonstrated efficient *in vitro* inhibition of cellular mechanisms involving EPAC1 in pathological cardiac conditions (Bisserier et al., 2014; Laurent et al., 2015; Zhang et al., 2019). In particular, it has recently shown promising *in vivo* activity on C57BL/6 mouse models of atrial/ventricular arrhythmias (Prajapati et al., 2019). However, we have previously shown that this molecule is prone to metabolization, especially enzymatic hydrolysis in mice plasma (Toussaint et al., 2021). The generated metabolite from hydrolysis (=N-deformylated-CE3F4) was shown to be inactive on EPAC1 (Courilleau et al., 2012). Only paraoxon, a pesticide known as a hydrolase inhibitor, has been identified to prevent (*R*)-CE3F4's degradation, but due to its toxicity it cannot be co-administrated to stabilize (*R*)-CE3F4 *in vivo*. Thus, the CE3F4 requires a specific drug delivery strategy to protect it against enzymatic degradation to investigate its full potential *in vivo*.

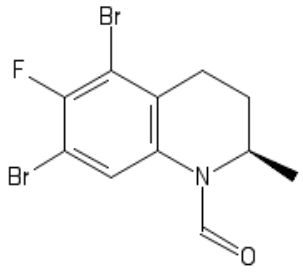

Figure 1. Structure of (*R*)-CE3F4.

Lipid-based nanosystems such as liposomes or lipid nanocapsules are relevant candidates for this purpose. They have been used for the encapsulation of a wide range of active molecules and have been proven safe due to their biocompatibility. Both can be tailored for multiple functions including by ligands fort site-specific targeting (Uster et al., 1996; Hoarau et al., 2004; Perrier et al., 2010; Cosco et al., 2017; Alshaer et al., 2018). In this work, we investigated the encapsulation of (*R*)-CE3F4 in liposomes and lipid nanocapsules, their potential for the protection of the molecule against enzymatic degradation in plasma *in vitro,* and the *in vivo* fate of the most promising combination after intravenous administration to mice.

2. *Materials & methods*

2.1. *Chemicals*

A racemic mixture of CE3F4 was synthesized using published procedures (Bouyssou et al., 1992). The active enantiomer (*R*)-CE3F4 was isolated with a purity >99% and enantiomeric excess (ee) >98% by applying the racemic mixture to a 250 × 30 mm Chiralpak® IB column (Daicel Corporation, Japan) equilibrated with n-hexane/propan-2-ol (95:5, v/v) at 42 mL/min. Paraoxon-ethyl with the analytical standard grade (paraoxon), Solutol® HS 15, D-α-Tocopheryl polyethylene glycol 1000 succinate (TPGS), 4-(dodecyloxy)benzoic acid (DOBA), polyethylene glycol 200 Da (PEG_{200}), ethylenediaminetetraacetic acid disodium salt dihydrate (EDTA) with a purity >99%, phosphate-buffered saline (PBS) at pH 7.4 (sterile and suitable for cell culture) were purchased from Sigma-Aldrich (Saint-Louis, MO, USA). L-α-phosphatidylcholine from egg (EggPC), L-α-phosphatidylcholine from Soy (HSPC), cholesterol (Chol), 1,2-distearoyl-sn-glycero-3-phosphoethanolamine-N-[methoxy(polyethyleneglycol)-2000] (DSPE-PEG_{2000}) were obtained from Avanti. Miglyol® 812 was purchased from Sasol (Johannesburg, South Africa). Zoletil® 50 (tiletamine, zolazepam), Rompun® 2% (xylazine), Iso-Vet (isoflurane) were respectively purchased from Virbac (Carros, France), Bayer (Leverkusen, NRW, Germany), and Piramal Critical Care (Voorschoten, Netherlands). Ethanol and dimethyl sulfoxide (DMSO) were provided from VWR (Radnor, PA, USA). Acetonitrile (ACN) with HPLC grade, propan-2-ol (IPA), and chloroform were acquired from Carlo Erba Reagents (Val-de-Reuil, France). To get deionized water (H_2O), a Milli-Q water purifying system (Millipore, Milford, MA, USA) was used. Concerning radioactive materials, CE3F4 (with ^{3}H on formyl bond) solubilized in acetonitrile was kindly provided by the Institut des Sciences du Vivant Frederic-Joliot (Commissariat à l'Energie Atomique, Gif-sur-Yvette, France) with a specific activity of 7.14 Ci/mmol, and 1-oleoyl-2-linoleoyl-sn-glycero-3-phosphocholine [linolenic-1-^{14}C] (^{14}C-1-oleoyl-2-linoleoyl-

GPC) in ethanol:toluene mixture (1:1) was purchased form Isobio (Fleurus, Belgium) with a specific activity of 50-60 mCi/mmol. Hionic-Fluor and Ultima Gold™ (Packard, Rungis, France) were used as scintillating cocktails for radioactive analyses. Soluene-350® used to dissolve biological samples was obtained from Perkin-Elmer (Courtaboeuf, France). Hydrogen peroxide (H_2O_2) was purchased from Merck (Darmstadt, Germany).

All liquids other than pure water or PBS were handled with MICROMAN E positive displacement pipettes (Middleton, WI, USA) due to the viscosity of plasma samples and the use of organic solvents.

2.2. *(R)-CE3F4 quantification*

Quantification was performed with an in-house developed and validated method which is suitable for (*R*)-CE3F4 quantification in formulations, as well as in biological media (in this case, plasma). This method allowed the quantification of (*R*)-CE3F4 from 0.40 to 150 µg/mL (using 1/concentration² weighting factor for linear regression, y = a + bx), and the separation of (*R*)-CE3F4 from its main detectable metabolite, with no interference regardless of the excipients, anesthetics and anticoagulant molecules used.

2.2.1. *Chromatographic system*

Analyses were performed on a Waters HPLC system (Milford, MA, USA) equipped with a diode array detector (Waters 2996 PDA), an injector (Waters 717 plus Autosampler), and a quaternary pump (Waters 600 HPLC pump). An external heater/chiller for the column was used (GRACE Model 7956R, Columbia, MD, USA). The separation was performed on a XBridge C18 3.5 µm, 4.6 × 100 mm column (Waters) at 35°C. The mobile phase consisted of a mixture of water and acetonitrile (40:60, v/v) under isocratic mode at a flow rate of 1.0 mL/min. The wavelength of 250 nm was used to trace the chromatograms, and the quantitative signal was the chromatographic peak area.

2.2.2. *Sample treatment*

An extraction procedure was carried out using EtOH and ACN to solubilize (*R*)-CE3F4 from different samples (formulation assay, biological sample). In polypropylene microcentrifuge tubes, 50 µL of a sample containing (*R*)-CE3F4 was added to 50 µL EtOH, followed by a vortex-mixing step (10 seconds). Then 150 µL of acetonitrile was added, followed by a vortex-mixing step for 30 seconds. To finish, microcentrifuge tubes were centrifuged at 13,000 g for 10 minutes at room temperature to eliminate non-solubilized

compounds (i.e. excipients, salts, proteins), and 100 µL of the supernatant was collected in autosampler vials. 15 µL of the supernatant was injected into the chromatographic system.

In the case of (*R*)-CE3F4 quantification in formulations, an observation under an optical microscope was carried out to verify the absence of crystals in suspension within the various preparations before sample treatment. When crystals were present, they were eliminated by low-speed centrifugation (10 min; 10,000 g) to only evaluate the solubilized (*R*)-CE3F4 fraction. The formulations were then diluted to the tenth before undergoing the sample treatment mentioned above.

2.3. *(R)-CE3F4 encapsulation*

2.3.1. *Liposomes*

2.3.1.1. *Liposome preparation*

Liposomes were prepared by the thin-film hydration method. (*R*)-CE3F4 was incorporated simultaneously with lipids in the chloroform solution, with a constant total concentration of lipids (total = 25.0 mM) but various lipids proportions (**Table 1**, **Tables S1 and S2**). The mixture was dried at ambient temperature for 60 min using a rotary evaporator R-215 (Büchi, Switzerland). The obtained film was hydrated with PBS at room temperature, except when HSPC was used, in which case the hydration was performed at 60°C. Then multilamellar liposomes were extruded (Lipex^{TM}, Northern Lipids, Canada) 8 times through two polycarbonate membranes with 0.1 µm pore diameters (Nuclepore, Whatman plc, United Kingdom) at ambient temperature or 60°C for HSPC formulations. The membrane was able to retain crystallized, non-encapsulated (*R*)-CE3F4. After the extrusion step, Amicon® filters with a cut-off of 100 kDa (Millipore, Milford, MA, USA) were used to eliminate the non-encapsulated fraction of (*R*)-CE3F4 from the liposome suspension.

2.3.1.2. *Evaluation of drug encapsulation*

The lipid recovery was evaluated by assaying the phosphatidylcholine content using an enzymatic colorimetric kit (Phospholipids, BIOLABO SA, Maizy, France) according to the manufacturer's instructions. Then the total lipid concentration was calculated by the assumption that proportions of all lipids remained constant during the formulation process. The drug encapsulation efficiency (EE%), the lipids recovery (LR%), and the drug loading (DL%) were calculated as follows:

$$EE\ (\%) = 100 \times [CE3F4]_{final} / [CE3F4]_{initial} \quad (1)$$

$$LR\ (\%) = 100 \times [Lipids]_{final} / [Lipids]_{initial} \quad (2)$$

$$DL\ (\%) = 100 \times [CE3F4]_{final} / [Lipids]_{final} \quad (3)$$

Table 1. Proportions of (*R*)-CE3F4 and lipids used for CE3F4 encapsulation in liposomes**.**

Liposome formulation		EggPC	EggPC-Chol	HSPC	HSPC-Chol$_{medium}$	HSPC-Chol
[(*R*)-CE3F4] (mM)		2.85	2.85	2.85	2.85	2.85
[Lipids] (mM)		25.0	25.0	25.0	25.0	25.0
(*R*)-CE3F4/lipid ratio (mol/mol)		11.4%	11.4%	11.4%	11.4%	11.4%
Lipid molar composition (n/n$_{total\ lipids}$)	EggPC	94.7%	56.6%	-	-	-
	HSPC	-	-	94.7%	74.7%	56.6%
	Cholesterol	-	38.2%	-	20.0%	38.2%
	DSPE-PEG$_{2000}$	5.3%	5.3%	5.3%	5.3%	5.3%

Table 2. Proportions of (*R*)-CE3F4, lipids, and aqueous media for nanocapsules formulations. Differences compared to the LNC$_1$ formulation are highlighted in italics.

LNC formulations	LNC$_1$	LNC$_2$	LNC$_3$	LNC$_1$-CE3F4$_{High}$	LNC$_2$-CE3F4$_{High}$	LNC$_3$-CE3F4$_{High}$
Miglyol (w/w$_{Total\ lipids}$)	41.6%	41.6%	41.6%	41.6%	41.6%	41.6%
Solutol HS 15 (w/w$_{Total\ lipids}$)	51.9%	*39.0%*	51.9%	51.9%	*39.0%*	51.9%
EggPC (w/w$_{Total\ lipids}$)	6.5%	*19.4%*	6.5%	6.5%	*19.4%*	6.5%
m$_{PBS}$:m$_{Total\ lipids}$ before dilution	1.1:1	1.1:1	*2.1:1*	1.1:1	1.1:1	*2.1:1*
m$_{total\ lipids}$ (mg)	770	770	770	770	770	770
m$_{(R)\text{-CE3F4}}$ (mg)	5.0	5.0	5.0	*10*	*10*	*10*
(*R*)-CE3F4/lipid ratio (w/w)	0.65%	0.65%	0.65%	*1.30%*	*1.30%*	*1.30%*
Approximative volumes of lipids (mL)	0.77	0.77	0.77	0.77	0.77	0.77
Volume of PBS before cold dilution (mL)	0.85	0.85	1.62	0.85	0.85	1.62
Volume of cold PBS (mL)	3.88	3.88	3.11	3.88	3.88	3.11
Final volume (mL)	5.5	5.5	5.5	5.5	5.5	5.5
[CE3F4] concentration expected (µg/mL)	909	909	909	*1818*	*1818*	*1818*

2.3.2. *Encapsulation in lipid nanocapsules*

The method used for the preparation of lipid nanocapsules (LNC) consisted of a phase inversion process (Heurtault et al., 2002). PBS was used as an aqueous phase, and a mixture of Solutol®, EggPC, and Miglyol® as lipid phase. Both phases were mixed into a vial containing a magnet. The vial was put into a water bath, and three temperature cycles of heating/cooling between 55°C and 85 °C were applied. After reaching 85°C for the third time, the vial was cooled to 65°C and a dilution with cold PBS (5°C) was performed under magnetic stirring, leading to the spontaneous formation of lipid nanocapsules. For (*R*)-CE3F4 encapsulation, the molecule was dissolved into Miglyol® before the process. All formulation conditions are summarized in

Table 2. After the cold dilution step, the (*R*)-CE3F4 concentration was measured, and appropriate dilutions were performed for all formulas to obtain the final concentration of 625 µg/mL. The formula used for *in vivo* studies was filtered on a 0.22 µm PVDF filter (Millipore, Milford, MA, USA).

2.3.3. *Size and zeta potential measurements*

The particle average hydrodynamic diameter (D_H) was determined by dynamic light scattering (Zetasizer Nano ZS, Malvern Instruments Corp., Worcestershire, UK). Samples were diluted in PBS before the measurements in a disposable cuvette and analyzed at a backscatter angle of 173°. Polydispersity index (PDI) was used as an indicator of size distribution. Zeta potential (ζ) was measured in the same apparatus in a folded capillary cell after 30-fold dilution with pure water (ionic strength corresponding to 1/30 PBS).

2.3.4. *Calculation of (R)-CE3F4 surface density and content per particle*

The number of (*R*)-CE3F4 molecules per nanoparticle was estimated (**Eq. 4**) as well as the potential surface density of (*R*)-CE3F4 (**Eq. 5**) for EggPC-liposomes, HSPC-liposomes, LNC_1, and LNC_1-$CE3F4_{High}$. The number of particles was estimated (**Eq. 6**) by dividing the virtual surface made of all surfactants "$S_{virtual}$" (**Eq. 7**) by the surface of one particle "$S_{particle}$" (**Figure S1**), the latter being calculated from the hydrodynamic diameter (D_H). For $S_{particle}$, one surface must be considered for LNC, but the two surfaces of the bilayer must be estimated for liposomes (inner and outer surfaces). The properties of the surfactants used for the calculation of $S_{virtual}$ are displayed in **Table S3**. All calculations were made for 1 mL

of formulation, considering the molar content of each surfactant and the lipids recovery (as measured in the case of liposomes; assumed to be 100% in the case of LNCs due to the one-pot process). Assumptions were made for particles surfaces calculations based on measured D_H. For liposomes, the obtention of unilamellar structures was assumed, the impact of acyl chains lengths of DSPE-PEG_{2000} on bilayer thickness was neglected due to its small molar proportion (near 5%). For LNCs, the polymer thickness related to PEG-HS was not taken into account due to the lack of conformational information on PEG 660 at high surface concentration.

$$\text{Number of CE3F4 per particle} = n_{CE3F4} \times N_A / \text{Number of particles} \quad (4)$$

with N_A: Avogadro number

$$\text{Surface density of CE3F4} = n_{CE3F4} \times N_A / S_{virtual} \quad (5)$$

$$\text{Number of particles} = S_{virtual} / S_{particle} \quad (6)$$

with $S_{particle}$ detailed in **Fig. S1**

$$S_{virtual} = (n_{tensioactive\ 1} \times a_{tensioactive\ 1} + n_{tensioactive\ 2} \times a_{tensioactive\ 2} + \ldots + n_{tensioactive\ n} \times a_{tensioactive\ n}) \times N_A \quad (7)$$

with a: area of the tensioactive's polar headgroup

2.4. *Vehicle for in vivo administration of free (R)-CE3F4*

The combination of Solutol HS 15, $PEG_{200,}$ and PBS (4.5:1:15, $m_{PEG200}/m_{Solutol\ HS\ 15}/v_{PBS}$) was evaluated to solubilize (*R*)-CE3F4 at the targeted concentration of 625 µg/mL. Namely, for 1.0 mL of preparation, 0.625 mg of (*R*)-CE3F4 was dissolved in 225 mg of PEG_{200} at 40°C, then 50 mg of Solutol HS 15 was added (4.5:1:15, $m_{PEG200}/m_{Solutol\ HS\ 15}/v_{PBS}$), and the mixture was gently homogenized for 30 min at 40°C. After this step, 750 µL of PBS at 40°C was added and the formula was gently mixed 10 min at 40°C then 1h at room temperature. To evaluate the solubilization or recrystallization of (*R*)-CE3F4, the formulation was observed under an optical microscope after preparation and until 24 h at room temperature. The solution was filtered on a 0.22 µm PVDF filter (Millipore, Milford, MA, USA) and assayed as described in section 2.2 before injection for *in vivo* studies.

2.5. *(R)-CE3F4 stability study in murine plasma, evaluation of the impact of formulations*

Formulations were first diluted in PBS if necessary to obtain an (*R*)-CE3F4 concentration of 625 µg/mL, then a dilution in murine plasma was performed to obtain a concentration of 60 µg/mL. Samples were put into a rotary agitator at 37°C, and after 5 min to 26 h, they were treated as described in section 2.2.2 to quantify total (*R*)-CE3F4 (released and encapsulated) and its metabolite resulting from hydrolysis. For data representation and comparison between all formulations, a normalization of the data was made by the ratio between the measured (*R*)-CE3F4 concentration at each sampling time and the measured concentration at 5 minutes (**Eq. 8**).

$$\text{Relative concentration (\%) at time t} = 100 \times [CE3F4]_t/[CE3F4]_{5min} \quad (8)$$

2.6. *In vivo* studies

(*R*)-CE3F4 studies in healthy C57BL/6N mice were carried out according to the local ethical committee guidelines (agreement number APAFIS#5584-20 16050312271349 v4). 7-week-old C57BL/6N male mice were purchased from Envigo (France) and let for 1 week after shipping for adaptation before starting experiments. Mice were kept in a separate animal room under climate-controlled conditions with a 12 h light/dark cycle, housed in polystyrene cages containing wood shavings, and fed standard rodent chow and water *ad libitum*. In both studies, the (*R*)-CE3F4 concentration was assayed as described in section 2.2 and adjusted to 625 µg/mL with PBS for each formulation. The administrated dose was 5 mg/kg, corresponding to an administration of 200 µL for a 25 g mouse. Formulations were slowly intravenously injected via a retro-orbital sinus.

2.6.1. *Pharmacokinetic study*

The study was designed with two groups, treated with free (*R*)-CE3F4 or (*R*)-CE3F4 encapsulated in LNC, and followed on 24 h (sampling times: 5 min, 15 min, 30 min, 1 h, 2 h, 3 h, 6 h, and 24 h). Three mice were used per group (each sampling time). In microcentrifuge tubes containing 30 µL of paraoxon solution (10^{-3} M, in DMSO), 300 µL of blood were collected by cardiac puncture with EDTA-coated needles. After gently mixing the sample, centrifugation was performed for 5 min at 10,000 g. 50 µL of the supernatant was processed as detailed in section 2.2.2, and then analyzed.

2.6.2. ***Biodistribution study***

2.6.2.1. *Design of the study*

Two groups were treated with free ^{3}H-CE3F4 or ^{3}H-CE3F4 in ^{14}C-LNC, and studied on 24 h with sampling times at 10 min, 15 min, 30 min, 1 h, 4 h, and 24 h. Three mice were used per group (each sampling time). Before the experiment, all mice were weighed. For each sampling time, heart, liver (including gallbladder), spleen, kidneys, and blood were collected and analyzed. Organ sampling occurred after a cardiac puncture with EDTA-coated needles allowing blood sampling. Blood and the totality of these organs were analyzed after sample treatment using a liquid scintillation counter (Model LS 6000 TA, Beckman, France), allowing the simultaneous quantification of ^{3}H and ^{14}C.

2.6.2.2. *Free ^{3}H-CE3F4*

Radiolabeled ^{3}H-CE3F4 in ACN was evaporated to dryness at room temperature under a stream of nitrogen in a 20 mL glass vial, then non-radioactive CE3F4 was added. ^{3}H-CE3F4 and CE3F4 were solubilized as described above for free CE3F4 to obtain a total concentration of 625 g/mL and a tritium concentration of 4.0 µCi/mL. Then the formulation was filtered through a 0.22 µm filter. For each mouse, 0.80 µCi of ^{3}H were injected.

2.6.2.3. *^{3}H-CE3F4 in ^{14}C-LNC*

Radiolabeled ^{3}H-CE3F4 in ACN and ^{14}C-1-oleoyl-2-linoleoyl-GPC in EtOH:toluene were evaporated to dryness at room temperature under a stream of nitrogen in a 20 mL glass vial, and non-radioactive (*R*)-CE3F4 was added. The dry residue was reconstituted with Miglyol at first, then encapsulation according to the LNC_1 formulation was performed to obtain a total CE3F4 concentration of 625 g/mL, a ^{3}H and a ^{14}C radioactive concentrations of 4.0 and 0.4 µCi/mL respectively. The preparation was then filtered through a 0.22 µm filter. For each mouse, 1 µCi of ^{3}H and 0.1 µCi of ^{14}C were injected.

2.6.2.4. *Sample treatment*

100 µL of blood were added to 400 µL of a mixture of Soluene-350®:IPA (1:1) and incubated for 30 min at 50°C, then a decolorization step of the sample with H_2O_2 (drop-to-drop addition) was done, and 4 mL of Hionic-Fluor was finally added as a scintillating liquid. The sample was vortexed before the analysis.

The totality of the organs (heart, kidneys, spleen, liver) was analyzed. After weighing, each organ was cut into small pieces, which were mixed with 2 mL Soluene-350® and incubated at 50°C overnight for tissue digestion. H_2O_2 was added (drop-to-drop) until decolorization, 16 mL of Ultima Gold™ scintillating liquid was added before vortex mixing, and then treated samples were analyzed.

2.6.2.5. *Data analysis*

Radioactivity for each organ was expressed in percentage of the injected dose, by dividing the number of disintegrations per minute (DPM) measured on the whole organ after digestion by the injected DPM. In the case of blood, the total blood volume of the mouse was approximated as a function of its weight (K = 0.072 mL/g) (Diehl et al., 2001), and the total activity corresponding to the whole blood was obtained according to **Eq. 9**.

$$\text{Activity}_{\text{whole blood}} = (\text{Activity}_{\text{blood sample}} / \text{Volume}_{\text{blood sample}}) \times K \times \text{mouse weight.} \quad (9)$$

The total radioactivity measured in all investigated tissues was calculated as the sum of each organ and total blood activities per mouse. Additionally, the ponderation of the activity by the mass of tissue analyzed was used to highlight differences in biodistribution between groups.

2.7. ***Statistical analysis***

All data were processed in GraphPad Prism (GraphPad Software, San Diego, CA, USA). Values are expressed as their mean ± standard deviation (µ ± S.D.). When comparing multiple groups, two-way ANOVA was applied with Bonferroni's multiple comparisons test. The statistical data were considered significant at $p < 0.05$ (*), 0.01 (**), 0.001 (***).

3. ***Results & Discussion***

3.1. *(R)-CE3F4 encapsulation*

3.1.1. *Liposomes*

The encapsulation of (*R*)-CE3F4 was investigated in liposomes prepared from HSPC or EggPC as main phospholipids, using various proportions of cholesterol. The type of phospholipid and the presence or not of cholesterol induced a significant effect on the amount of (*R*)-CE3F4 encapsulated (**Figure 2**), whereas the hydrodynamic diameter and the zeta potential remained relatively unchanged among formulations (**Table 3**). Maximal (*R*)-CE3F4 encapsulation (EE > 80%) and lipid recovery (LR > 80%) were obtained for EggPC liposomes without cholesterol, resulting in a drug loading (DL) of 11 % (mol/mol). In detail, **Figure 2** and a two-way ANOVA analysis show a moderate impact of the phospholipid on EE (with HSPC being less favorable than EggPC), as well as a negative impact of cholesterol on EE. A significant interaction was found between both parameters, resulting in a drop of (*R*)-CE3F4 encapsulation in liposomes prepared from HSPC and cholesterol. In this case, the measured (*R*)-CE3F4 concentration in the formulation was by far the lowest and close to the observed (*R*)-CE3F4 solubility in PBS (~ 40 µM). The investigation of an intermediate cholesterol proportion in HSPC liposomes confirmed the negative correlation between cholesterol and EE when this lipid is used (**Figure S2**). Other liposomal formulations containing DOBA or TPGS in their lipid composition also showed a negative impact of cholesterol on EE (**Tables S4 and S5**). Altogether, these results suggest a competition in their insertion within the liposome bilayer between cholesterol and (*R*)-CE3F4, combined with an influence of the membrane fluidity related to differences between phase transition temperature of EggPC and HSPC which are respectively near -10°C (Amselem et al., 1995) and 52°C (Horowitz et al., 1992), and the influence of cholesterol (Ohvo-Rekilä et al., 2002; Halling et al., 2008). The interaction between CE3F4 and micelles of Triton X-100 has been recently reported, with the exposure of the CE3F4's formyl moiety at the surface of the micelles while the hydrophobic part interacts with the aromatic ring and the hydrocarbon chain of Triton X-100 (Boulton et al., 2019). Regarding cholesterol location in bilayers, it is known that its hydroxyl group is exposed at the surface of the bilayer (in interaction with polar heads of phospholipids) while its hydrophobic parts (steroid core and hydrocarbon chain) interact with the hydrophobic tail of phospholipids (Ohvo-Rekilä et al., 2002). The competition between cholesterol and another apolar molecule (celecoxib) which also interacts with polar heads of phospholipids in liposome bilayer has already been described (Deniz et al., 2010). Indeed, the authors reported a lower celecoxib EE when cholesterol was added in large molar proportion (33%) in liposomes. Thus, according to our results and the literature, a

competition between cholesterol and the CE3F4 in their location in bilayer membrane seems the most probable hypothesis. Despite this, (*R*)-CE3F4 was successfully encapsulated with satisfactory EE in at least three different liposomal formulations (EggPC, HSPC, and EggPC-Chol), which were further evaluated for their ability to protect (*R*)-CE3F4 from degradation in murine plasma.

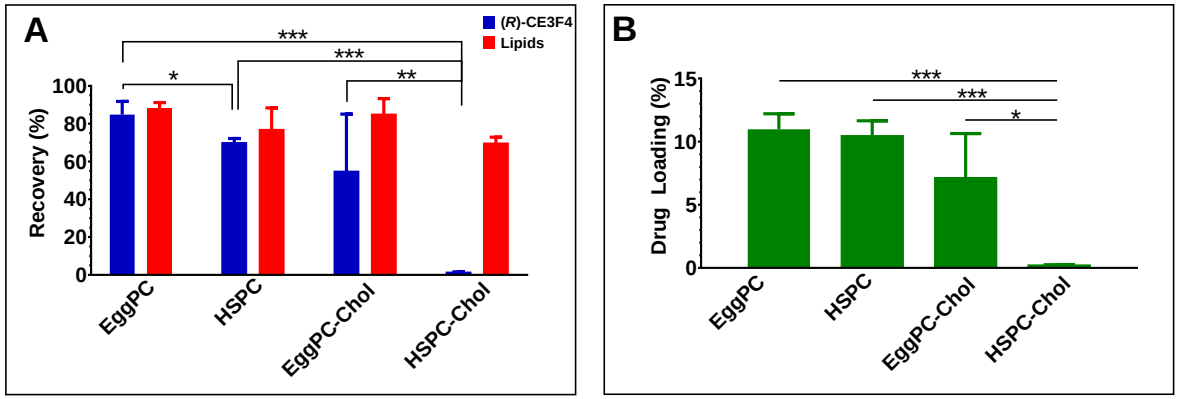

Figure 2. (A) (*R*)-CE3F4 encapsulation efficiency (EE, blue) and lipid recovery (LR, red) for liposomes prepared from EggPC or HSPC, with or without cholesterol. (B) Drug loading (mol/mol) achieved with liposomes. n = 3 per formulation group; p-value < 0.05 (*), 0.01 (**), 0.001 (***).

Table 3. Colloidal properties of liposomes investigated for (*R*)-CE3F4 encapsulation (mean ± S.D., n = 3).

Formulation	EggPC	EggPC-Chol	HSPC	HSPC-Chol
Hydrodynamic diameter (nm)	90 ± 11	97 ± 11	106 ± 4	98 ± 6
Polydispersity index	0.067 ± 0.036	0.045 ± 0.023	0.082 ± 0.12	0.056 ± 0.003
ζ potential (mV)	-19.1 ± 3.0	-19.8 ± 4.4	-17.2 ± 3.7	-14.1 ± 0.9

3.1.2. ***Lipid nanocapsules***

Lipid nanocapsules (LNC) suspensions were obtained by mixing the Miglyol oil, containing dissolved (*R*)-CE3F4, with EggPC and Solutol HS15 in an aqueous medium. Unlike liposomes, this process consists of a one-pot mixing (no transfer, extrusion, or purification steps involved), alleviating the risk of drug or excipient loss. Excipients proportions were based on a reference

LNC formulation (Heurtault et al., 2002), named LNC_1 in the following. Other proportions within the domain of LNC formation were explored by altering the EggPC/Solutol ratio and the aqueous phase initial fraction (LNC_2, LNC_3). Two initial amounts of (*R*)-CE3F4 (5 mg for LNC_{1-3};10 mg for LNC_{1-3}-$CE3F4_{High}$) were studied for a constant amount of lipids (770 mg) to evaluate the impact of the CE3F4:lipids ratio (w/w). The theoretical drug loading was therefore 0.65% (w/w) for LNC_{1-3} and 1.30% for LNC_{1-3}-$CE3F4_{High}$.

Homogeneous colloidal suspensions were obtained in all cases, with hydrodynamic diameters around 30 nm and polydispersity indexes below 0.2 (**Table 4**). Notably, despite using (*R*)-CE3F4 concentrations more than a hundred-times above its solubility in PBS for all LNC formulations, optical microscopy observations indicated an absence of crystals in suspension, which was confirmed by the assessment of (*R*)-CE3F4 concentration after low-speed centrifugation as well as after filtration through a 0.2 µm filter (for example, (*R*)-CE3F4 recovery after the whole process was 101.8% ± 4.6% (n = 3) for LNC_1), indicating a correct encapsulation of the (*R*)-CE3F4 in LNCs. When the initial (*R*)-CE3F4 amount was doubled (LNC_{1-3}-$CE3F4_{High}$), this modification did not alter the formulation process, allowing high drug concentrations in the final LNC suspensions, up to 2 orders of magnitude higher than its PBS solubility and twice as much as in liposomes (**Table 4**). Compared to liposomes, the diameter is small enough to allow a 0.2 µm filtration as an easy sterilization process before *in vivo* studies.

Table 4. Colloidal properties of LNC suspensions prepared in presence of (*R*)-CE3F4, and drug concentrations achieved in the preparation (n=1-3).

LNC formulations	LNC_1	LNC_2	LNC_3	LNC_1-$CE3F4_{High}$	LNC_2-$CE3F4_{High}$	LNC_3-$CE3F4_{High}$
Hydrodynamic diameter (nm)	29.3 ± 0.6	28.4	30.6	29.6	27.8	30.9
Polydispersity index	0.04 ± 0.01	0.16	0.03	0.09	0.16	0.09
[CE3F4] (µg/mL)	897.9 ± 21.9	910.1	917.7	1737	1766	1772
CE3F4 recovery (%)	98.8 ± 2.4	100%	101%	96%	97%	97%

Drug loading (% w/w)	0.64 ± 0.02	0.65%	0.66%	1.24%	1.26%	1.27%

3.2. *(R)-CE3F4 protection in plasma*

A plasmatic half-life of 39.9 min was previously reported for (*R*)-CE3F4 (confidence interval 95%: from 36.9 to 43.4 min) (Toussaint et al., 2021). The disappearance of (*R*)-CE3F4 in C57BL/6N mice plasma *in vitro* can be represented by a one-phase exponential decay for all formulation as shown in **Figure 3**. Results show unambiguously that liposomes do not confer any protection to (*R*)-CE3F4 from plasmatic degradation *in vitro*, with degradation kinetics similar to free (*R*)-CE3F4, suggesting a rapid release from the liposomes, or at least an insufficient protection from accessibility to enzymes. Other liposome formulations using TPGS or DOBA did not show any improvement either **(Tables S4 and S5)**. In contrast, LNC formulations increased (*R*)-CE3F4 apparent half-life by at least 2.7-fold (LNC_2-$CE3F4_{High}$) and up to 5.9-fold (LNC_1). The protection effect was higher for $LNC_{1\text{-}3}$ compared to $LNC_{1\text{-}3}$-$CE3F4_{High}$, showing the importance of the initial CE3F4-to-lipids ratio. A higher or faster drug release in the case of LNCs loaded with higher amounts of (*R*)-CE3F4 could explain this difference.

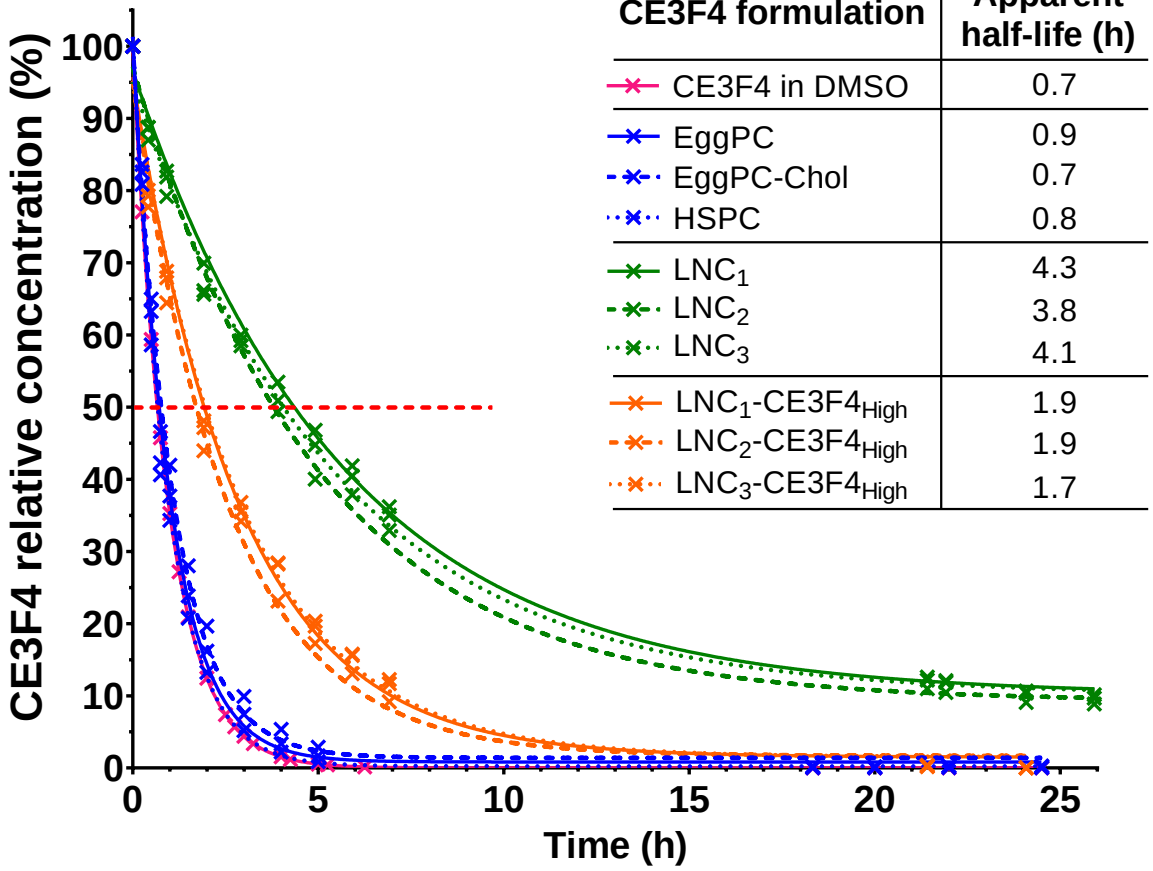

CE3F4 formulation	Apparent half-life (h)
CE3F4 in DMSO	0.7
EggPC	0.9
EggPC-Chol	0.7
HSPC	0.8
LNC_1	4.3
LNC_2	3.8
LNC_3	4.1
LNC_1-$CE3F4_{High}$	1.9
LNC_2-$CE3F4_{High}$	1.9
LNC_3-$CE3F4_{High}$	1.7

Figure 3. *In vitro* degradation kinetics of (*R*)-CE3F4 encapsulated in liposomes (EggPC, EggPC-Chol, HSPC), in lipid nanocapsules (LNC_1 to LNC_3, and LNC_1-$CE3F4_{High}$ to LNC_3-$CE3F4_{High}$), compared to free CE3F4 solubilized in DMSO, in C57BL/6N mice plasma. 50% of degradation is shown by a red dotted line. Detailed apparent half-lives are reported in the associated table. In all cases, the determination coefficient was higher than 0.99.

A possible hypothesis accounting for these discrepancies of drug protection towards degradation could be a different accessibility of the drug molecules at the surface of the nanocarriers. Because liposomes and LNCs have notable differences in terms of particle size and drug loading, the number of (*R*)-CE3F4 molecules per nanoparticle surface was estimated (**Table S6**). The differences in the values calculated for liposomes (0.18-0.23 molecules/nm^2) and LNCs (0.09-0.16 molecules/nm^2) might not be enough to account for the protection effect observed experimentally. A more pronounced gap was found in terms of number of (*R*)-CE3F4 molecules per nanoparticle (0.7-1.3×10^4 molecules/particle for liposomes, 2-4×10^2 for LNCs), suggesting a higher or faster drug realease in the case of liposomes driven by a higher drug concentration gradient than in the case of LNCs. While further studies on the structural oraganization of CE3F4 within each type of nanocarrier by differential scanning calorimetry and small angle X-ray scattering may provide additional insight, the LNC_1 formulation was selected based on the present observations for further *in vivo* evaluation of (*R*)-CE3F4 delivery.

3.3. *(R)-CE3F4 fate in vivo*

3.3.1. *Vehicle choice for the administration of free (R)-CE3F4*

Prajapati et al. already use DMSO 30% (in water) to solubilize (*R*)-CE3F4 for *in vivo* studies (Prajapati et al., 2019). However, in these conditions, we observed the recrystallization of (*R*)-CE3F4 at ambient temperature in less than 18 h, which does not allow the use of 30% DMSO for studies in animals over 24 h (data not shown). Because the use of DMSO with a proportion larger than 30% (v/v) is not recommended (Thackaberry et al., 2014), we explored the interest of Solutol HS 15 and PEG_{200} to solubilize (*R*)-CE3F4 in PBS at the target concentration of 625 µg/mL. No recrystallization was observed during at least 24 h. The sterilization through a 0.22 µm filter confirmed the solubilization of the drug, and allowed the use of the selected formulation for pharmacokinetic and biodistribution studies as the control group.

3.3.2. *Pharmacokinetic study*

In this study, paraoxon was used as metabolism inhibitor in murine plasma to stop the enzymatic degradation of (*R*)-CE3F4 that may occur between blood sampling and protein precipitation before HPLC analysis. A very fast disappearance of (*R*)-CE3F4 was observed for the two groups (free CE3F4 and LNC). Indeed, the (*R*)-CE3F4 concentration measured was less than 2.0% of the maximal expected concentration in the

bloodstream (~ 62.5 µg/mL) at 5 min. After 15 min, the (*R*)-CE3F4 signal was below the limit of quantification (i.e. 0.40 µg/mL, corresponding to 0.6% of the maximal expected concentration) despite the LNC use (**Table 5**).

Table 5. Measured plasma concentration of (*R*)-CE3F4 during pharmacokinetic study on C57BL/6N mice injected with free (*R*)-CE3F4 or (*R*)-CE3F4 encapsulated in lipid nanocapsules (LNC). < LOQ: signal below lower limit of calibration curve (0.40 µg/mL).

Group	Sampling times		
	5 min	15 min	from 30 min to 24 h
Free CE3F4 (µg/mL)	0.43	< LOQ	< LOQ
CE3F4 in LNC (µg/mL)	1.30 ± 0.70	0.43 ± 0.07	< LOQ

This rapid clearance of free (*R*)-CE3F4 from the plasma is consistent with the rapid metabolization shown *in vitro* in murine plasma, mostly by hydrolysis of (*R*)-CE3F4 by enzymes in plasma as previously reported by our team (Toussaint et al., 2021). However, the main metabolite identified *in vitro* was not observed here *in vivo* using a similar HPLC-UV analysis, questioning hydrolysis as the main metabolism pathway, even though secondary products cannot be excluded. Other factors could explain the rapid clearance of free (*R*)-CE3F4, such as a fast distribution outside the plasma compartment, into tissues or blood cells (which are eliminated during sample treatment), a fast elimination, or a combination of these different possibilities.

Despite promising results reported *in vitro* (section 3.2), it appeared that the formulation of (*R*)-CE3F4 with LNCs did not improve its pharmacokinetic profile. This could be explained by a faster drug release *in vivo* driven by conditions not encountered *in vitro*, such as sequestration in tissues or blood constituents. Another possibility is a stable entrapment in LNCs, which are rapidly cleared from the plasma.

3.3.3. *Biodistribution studies*

To go deeper in the understanding of the fate of (*R*)-CE3F4 *in vivo*, the biodistribution was investigated using ^{3}H-CE3F4 as a tracer. A ^{14}C-lipid was also added in the LNC formulation to monitor the fate of the nanocarrier simultaneously. The impact of sterilizing by filtration was first

investigated. The activities of ^{3}H and ^{14}C measured after filtration were respectively 98.5% and 97.7% of the initial values, and the observed ratio $^{3}H/^{14}C$ in the formulation remained stable (8.95 before vs. 9.02 after filtration). These results confirm the easy sterilization of CE3F4 formulated as LNCs.

The biodistribution of free ^{3}H-CE3F4 (**Figure 4A**) and ^{3}H-CE3F4 delivered with LNCs (**Figure 4B**) showed similar trends with slight differences. Ten minutes after injection of free CE3F4, less than 5 % of the injected tritium was found in the blood, with some distribution to liver and kidneys, then plateauing or decreasing. This is consistent with the rapid clearance from the plasma compartment described above and supports a rapid elimination rather than any accumulation in the investigated tissues. In the case of CE3F4 delivered with LNCs, no significant differences in the fractions of injected doses were measured, suggesting a rapid release of CE3F4 from LNCs and a similar distribution compared to free CE3F4. A slight increase in drug amount can still be noticed in the liver in the first hour. This last observation is confirmed when correcting the measured ^{3}H activities by the organ weight (**Figure 4C**), which shows a higher CE3F4 presence in the liver tissue when delivered with LNCs, probably due to the accumulation of LNCs in the liver.

It can be noted that all organs exhibit a similar activity at 24 h (25-60 DPM/mg of tissue). This could be explained by the hydrolysis of the formamide bond of CE3F4 by plasmatic enzymes in rodents (Gleason and Vogh, 1971; Takenaga et al., 1998; Toussaint et al., 2021). This would produce ^{3}H-formic acid, which is known to react with macromolecules, to be metabolized as $CO_2 + H_2O$, or to be directly eliminated in urines (Thompson, 1992), altering a proper evaluation of CE3F4 biodistribution with unwanted signal correlated to formic acid distribution.

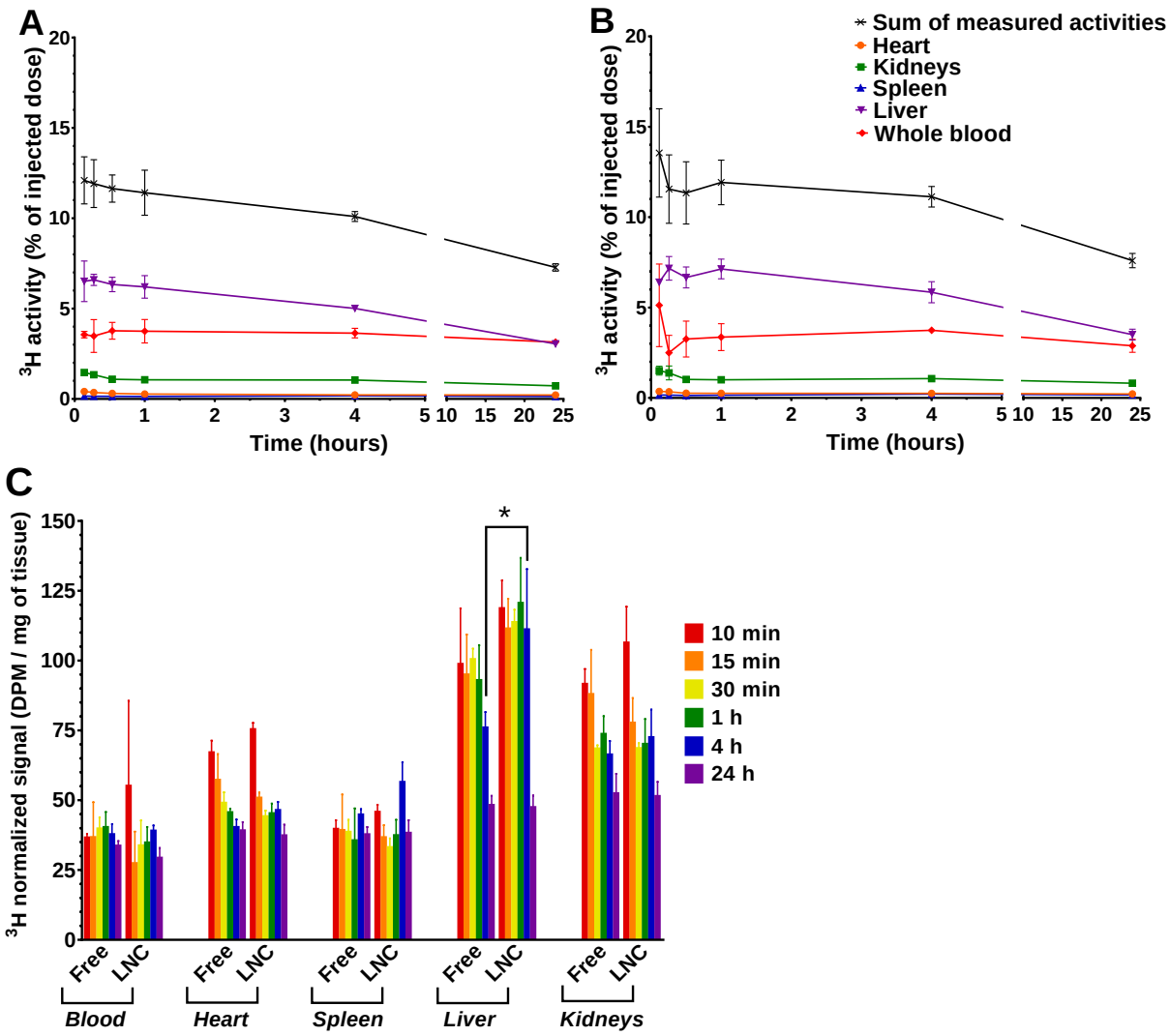
A
B
C
^{3}H activity (% of injected dose)
Time (hours)
Sum of measured activities
Heart
Kidneys
Spleen
Liver
Whole blood
^{3}H normalized signal (DPM / mg of tissue)
10 min
15 min
30 min
1 h
4 h
24 h
Free
LNC
Blood
Heart
Spleen
Liver
Kidneys
*

Figure 4. Biodistribution of ^{3}H in different organs is expressed as a percentage of the injected dose (A, B). (A) Free ^{3}H-CE3F4 and (B) ^{3}H-CE3F4 formulated with ^{14}C-LNCs were injected intravenously into C57BL/6N mice. (C) ^{3}H distribution in organs corrected by the mass of each organ, for free ^{3}H-CE3F4 and ^{3}H-CE3F4 delivered with LNCs. P-value < 0.05 (*).

The simultaneous labeling of ^{3}H-CE3F4 and ^{14}C-LNC (using a ^{14}C-phospholipid as a tracer of LNCs) allowed us to investigate the fate of these nanocarriers and to compare it with the (*R*)-CE3F4's. First, we can observe in **Figure 5** that the ^{14}C biodistribution profile is very different from the tritium biodistribution profile, with still 84% of the injected dose recovered at 10 min, overwhelmingly recovered in the blood compartment (72% of the injected dose), and distribution to the liver which becomes the main distribution compartment after 3 h. The mean half-life in blood was 1.4 h (confidence interval 95%: [0.8 to 5.0]), which is consistent with a previous study using radiolabeled LNC (Lacoeuille et al., 2007). The liver uptake of ^{14}C-LNC could explain the slight increase in liver uptake of ^{3}H-CE3F4 administered as LNC formulation (**Figure 4**C). Furthermore, as reported in **Table 6**, the ^{3}H-to-^{14}C ratio in blood samples dropped from its initial value of 9.02 in the formulation to 0.88 ± 0.49 after 10 min, down to a minimum of 0.37 ± 0.17 after 15 min, showing a fast release of ^{3}H-CE3F4 from ^{14}C-LNC. Thus, these results on ^{3}H-CE3F4 and ^{14}C-LNC biodistributions show that a small fraction of CE3F4 administered as LNCs is delivered to the liver with the nanocarriers, while the rest of the drug is rapidly released and follows the same fate as free CE3F4.

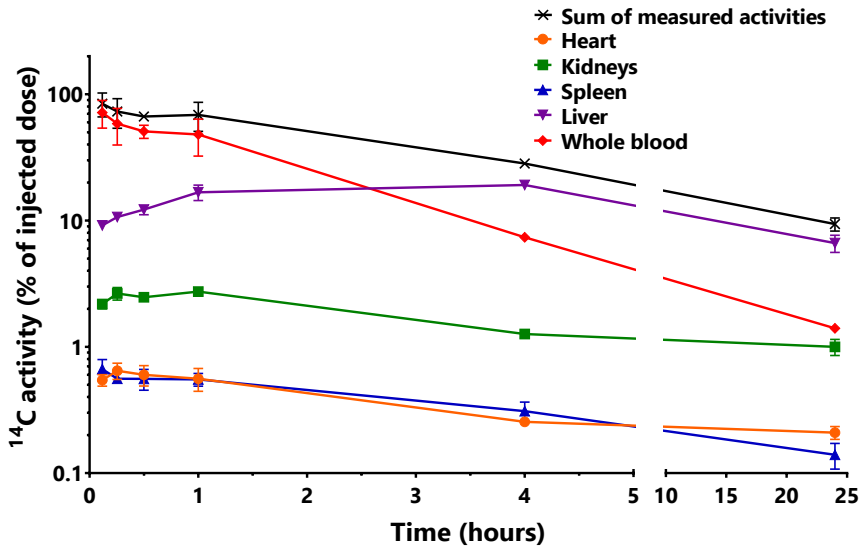

Figure 5. Biodistribution of ^{14}C in different organs is expressed as the percentage of the injected dose. ^{3}H-CE3F4 in ^{14}C-LNC formulation was injected into C57BL/6N mice.

Table 6. Kinetics of $^{3}H/^{14}C$ ratio in healthy C57BL/6 mice from the LNC formulation intravenously injected to blood samples analyzed.

Analyzed samples	Time (h)	Ratio $^{3}H/^{14}C$
LNC-formulation	Initial ratio "t=0"	9.02
Blood samples	0.17	0.88 ± 0.49
	0.25	0.37 ± 0.17
	0.5	0.63 ± 0.25
	1.0	0.69 ± 0.09

4. *Conclusions*

To our knowledge, this is the first study describing the pharmacokinetics and biodistribution of the (*R*)-CE3F4 drug candidate, and its formulation with nanocarriers to modulate its stability and delivery. (*R*)-CE3F4 was successfully encapsulated in liposomes and LNCs, and these lipid-based nanocarriers increased its apparent solubility by up to two orders of magnitude compared to its solubility in water. An interaction between the drug and cholesterol within liposomes has been unveiled, and its nature remains to be elucidated. Only LNCs were found to offer significant protection of (*R*)-CE3F4 from degradation, which could be due to a different structural organization compared to liposomes, in addition to be compatible with sterilizing filtration, making these nanocarriers the most suitable candidates for *in vivo* administration. In addition, LNCs obtained by the phase-inversion process can been administrated among a large choice of routes [injectable (Lacoeuille et al., 2007; Allard et al., 2009; Hureaux et al., 2010; Groo et al., 2015; Sasso et al., 2016; Resnier et al., 2017; Lollo et al., 2018), oral (Peltier et al., 2006; Ramadan et al., 2011; Amara et al., 2018; Ashour et al., 2020), pulmonary (Hureaux et al., 2009), dermal (El-Sheridy et al., 2019; Hatahet et al., 2017), intranasal (Mohsen et al., 2020), ocular (Eldesouky et al., 2021)], some of which are compatible with long-term administration as needed to treat chronic cardiovasculaire diseases (e.g. heart failure, hypertension). However few studies using LNC have focused on the formulation of compounds treating the cardiovascular system (Lamprecht et al., 2002; Mohsen et al., 2020). While the described LNC formulations did not significantly improve the drug pharmacokinetic profile after intravenous administration to mice, this study provides new fundamental data on the (*R*)-CE3F4 behavior *in vivo*. Thus, essential foundations have been laid for the development of future formulations aiming at improving (*R*)-CE3F4 delivery.

Acknowledgment

The “Institut Galien Paris-Sud” and the “Service de Chimie Bioorganique et de Marquage” belong to the Laboratory of Excellence in Research on Medication and Innovative Therapeutics (ANR-10-LABX-0033-LERMIT). We thank Mrs Assia Hessani for technical assistance in the radioactivity assay.

Conflict of Interest

The authors declare no conflict of interest regarding this publication.

References

Allard, E., Jarnet, D., Vessières, A., Vinchon-Petit, S., Jaouen, G., Benoit, J.-P., Passirani, C., 2009. Local Delivery of Ferrociphenol Lipid Nanocapsules Followed by External Radiotherapy as a Synergistic Treatment Against Intracranial 9L Glioma Xenograft. Pharm. Res. 27, 56. https://doi.org/10.1007/s11095-009-0006-0

Alshaer, W., Hillaireau, H., Vergnaud, J., Mura, S., Deloménie, C., Sauvage, F., Ismail, S., Fattal, E., 2018. Aptamer-guided siRNA-loaded nanomedicines for systemic gene silencing in CD-44 expressing murine triple-negative breast cancer model. J. Controlled Release 271, 98–106. https://doi.org/10.1016/j.jconrel.2017.12.022

Amara, R.O., Ramadan, A.A., El-Moslemany, R.M., Eissa, M.M., El-Azzouni, M.Z., El-Khordagui, L.K., 2018. Praziquantel–lipid nanocapsules: an oral nanotherapeutic with potential Schistosoma mansoni tegumental targeting. Int. J. Nanomedicine 13, 4493–4505. https://doi.org/10.2147/IJN.S167285

Amselem, S., Zawoznik, E., Yogev, A., Friedman, D., 1995. Emulsomes, a new type of lipid assembly., in: Barenholz, Y., Lasic, D.D. (Eds.), Handbook of Nonmedical Applications of Liposomes: From Design to Microreactors. CRC Press, pp. 209–223. https://doi.org/10.1201/9781351072724

Ashour, A.A., Ramadan, A.A., Abdelmonsif, D.A., El-Kamel, A.H., 2020. Enhanced oral bioavailability of Tanshinone IIA using lipid nanocapsules: Formulation, in-vitro appraisal and pharmacokinetics. Int. J. Pharm. 586, 119598. https://doi.org/10.1016/j.ijpharm.2020.119598

Bisserier, M., Blondeau, J.-P., Lezoualc'h, F., 2014. Epac proteins: specific ligands and role in cardiac remodelling. Biochem. Soc. Trans. 42, 257–264. https://doi.org/10.1042/BST20140033

Boulton, S., Selvaratnam, R., Ahmed, R., Van, K., Cheng, X., Melacini, G., 2019. Mechanisms of Specific versus Nonspecific Interactions of Aggregation-Prone Inhibitors and Attenuators. J. Med. Chem. https://doi.org/10.1021/acs.jmedchem.9b00258

Bouyssou, P., Goff, C.L., Chenault, J., 1992. Synthesis of 7- and 5,7-substituted-6-fluoro-2-methyl-1,2,3,4-tetrahydroquinolines: Convenient precursors of quinolone antibacterial agents. J. Heterocycl. Chem. 29, 895–898. https://doi.org/10.1002/jhet.5570290436

Cosco, D., Tsapis, N., Nascimento, T.L., Fresta, M., Chapron, D., Taverna, M., Arpicco, S., Fattal, E., 2017. Polysaccharide-coated liposomes by post-insertion of a hyaluronan-lipid conjugate. Colloids Surf. B Biointerfaces 158, 119–126. https://doi.org/10.1016/j.colsurfb.2017.06.029

Courilleau, D., Bisserier, M., Jullian, J.-C., Lucas, A., Bouyssou, P., Fischmeister, R., Blondeau, J.-P., Lezoualc'h, F., 2012. Identification of a tetrahydroquinoline analog as a pharmacological inhibitor of the cAMP-binding protein Epac. J. Biol. Chem. 287, 44192–44202.

Courilleau, D., Bouyssou, P., Fischmeister, R., Lezoualc'h, F., Blondeau, J.-P., 2013. The (R)-enantiomer of CE3F4 is a preferential inhibitor of human exchange protein directly activated by cyclic AMP isoform 1 (Epac1). Biochem. Biophys. Res. Commun. 440, 443–448.

Deniz, A., Sade, A., Severcan, F., Keskin, D., Tezcaner, A., Banerjee, S., 2010. Celecoxib-loaded liposomes: effect of cholesterol on encapsulation and in vitro release characteristics. Biosci. Rep. 30, 365–373. https://doi.org/10.1042/BSR20090104

Diehl, K.-H., Hull, R., Morton, D., Pfister, R., Rabemampianina, Y., Smith, D., Vidal, J.-M., Vorstenbosch, C.V.D., 2001. A good practice guide to the administration of substances and removal of blood, including routes and volumes. J. Appl. Toxicol. 21, 15–23. https://doi.org/10.1002/jat.727

Eldesouky, L.M., El-Moslemany, R.M., Ramadan, A.A., Morsi, M.H., Khalafallah, N.M., 2021. Cyclosporine Lipid Nanocapsules as Thermoresponsive Gel for Dry Eye Management: Promising Corneal Mucoadhesion, Biodistribution and Preclinical Efficacy in Rabbits. Pharmaceutics 13, 360. https://doi.org/10.3390/pharmaceutics13030360

El-Sheridy, N.A., Ramadan, A.A., Eid, A.A., El-Khordagui, L.K., 2019. Itraconazole lipid nanocapsules gel for dermatological applications: In vitro characteristics and treatment of induced cutaneous candidiasis. Colloids Surf. B Biointerfaces 181, 623–631. https://doi.org/10.1016/j.colsurfb.2019.05.057

Gleason, L.N., Vogh, B.P., 1971. Deformylation of 4,4'-diformamidodiphenyl sulfone (DFD) by plasma of certain mammals. Biochem. Pharmacol. 20, 2409–2416. https://doi.org/10.1016/0006-2952(71)90241-3

Groo, A., Bossiere, M., Trichard, L., Legras, P., Benoit, J., Lagarce, F., 2015. *In vivo* evaluation of paclitaxel-loaded lipid nanocapsules after intravenous and oral administration on resistant tumor. Nanomed. 10, 589–601. https://doi.org/10.2217/nnm.14.124

Halling, K.K., Ramstedt, B., Nyström, J.H., Slotte, J.P., Nyholm, T.K.M., 2008. Cholesterol Interactions with Fluid-Phase Phospholipids: Effect on the Lateral Organization of the Bilayer. Biophys. J. 95, 3861–3871. https://doi.org/10.1529/biophysj.108.133744

Hatahet, T., Morille, M., Shamseddin, A., Aubert-Pouëssel, A., Devoisselle, J.M., Bégu, S., 2017. Dermal quercetin lipid nanocapsules: Influence of the formulation on antioxidant activity and cellular protection against hydrogen peroxide. Int. J. Pharm. 518, 167–176. https://doi.org/10.1016/j.ijpharm.2016.12.043

Heurtault, B., Saulnier, P., Pech, B., Proust, J.-E., Benoit, J.-P., 2002. A novel phase inversion-based process for the preparation of lipid nanocarriers. Pharm. Res. 19, 875–880.

Hoarau, D., Delmas, P., David, S., Roux, E., Leroux, J.-C., 2004. Novel Long-Circulating Lipid Nanocapsules. Pharm. Res. 21, 1783–1789. https://doi.org/10.1023/B:PHAM.0000045229.87844.21

Horowitz, A.T., Barenholz, Y., Gabizon, A.A., 1992. In vitro cytotoxicity of liposome-encapsulated doxorubicin: dependence on liposome composition and drug release. Biochim. Biophys. Acta BBA - Biomembr. 1109, 203–209. https://doi.org/10.1016/0005-2736(92)90084-Y

Hothi, S.S., Gurung, I.S., Heathcote, J.C., Zhang, Y., Booth, S.W., Skepper, J.N., Grace, A.A., Huang, C.L.-H., 2008. Epac activation, altered calcium homeostasis and ventricular arrhythmogenesis in the murine heart. Pflüg. Arch. - Eur. J. Physiol. 457, 253–270. https://doi.org/10.1007/s00424-008-0508-3

Hureaux, J., Lagarce, F., Gagnadoux, F., Rousselet, M.-C., Moal, V., Urban, T., Benoit, J.-P., 2010. Toxicological Study and Efficacy of Blank and Paclitaxel-Loaded Lipid Nanocapsules After i.v. Administration in Mice. Pharm. Res. 27, 421–430. https://doi.org/10.1007/s11095-009-0024-y

Hureaux, J., Lagarce, F., Gagnadoux, F., Vecellio, L., Clavreul, A., Roger, E., Kempf, M., Racineux, J.-L., Diot, P., Benoit, J.-P., Urban, T., 2009. Lipid nanocapsules: ready-to-use nanovectors for the aerosol delivery of paclitaxel. Eur. J. Pharm. Biopharm. Off. J. Arbeitsgemeinschaft Pharm. Verfahrenstechnik EV 73, 239–246. https://doi.org/10.1016/j.ejpb.2009.06.013

Kumar, N., Gupta, S., Dabral, S., Singh, S., Sehrawat, S., 2017. Role of exchange protein directly activated by cAMP (EPAC1) in breast cancer cell migration and apoptosis. Mol. Cell. Biochem. 430, 115–125. https://doi.org/10.1007/s11010-017-2959-3

Lacoeuille, F., Hindre, F., Moal, F., Roux, J., Passirani, C., Couturier, O., Cales, P., Le Jeune, J.J., Lamprecht, A., Benoit, J.P., 2007. In vivo evaluation of lipid nanocapsules as a promising colloidal carrier for paclitaxel. Int. J. Pharm. 344, 143–149. https://doi.org/10.1016/j.ijpharm.2007.06.014

Lamprecht, A., Bouligand, Y., Benoit, J.-P., 2002. New lipid nanocapsules exhibit sustained release properties for amiodarone. J. Controlled Release 84, 59–68. https://doi.org/10.1016/S0168-3659(02)00258-4

Laurent, A.-C., Bisserier, M., Lucas, A., Tortosa, F., Roumieux, M., De Régibus, A., Swiader, A., Sainte-Marie, Y., Heymes, C., Vindis, C., Lezoualc'h, F., 2015. Exchange protein directly activated by cAMP 1 promotes autophagy during cardiomyocyte hypertrophy. Cardiovasc. Res. 105, 55–64.

Lollo, G., Ullio-Gamboa, G., Fuentes, E., Matha, K., Lautram, N., Benoit, J.-P., 2018. In vitro anti-cancer activity and pharmacokinetic evaluation of curcumin-loaded lipid nanocapsules. Mater. Sci. Eng. C 91, 859–867. https://doi.org/10.1016/j.msec.2018.06.014

Lorenz, R., Aleksic, T., Wagner, M., Adler, G., Weber, C., 2008. The cAMP/Epac1/Rap1 Pathway in Pancreatic Carcinoma. Pancreas 37, 102–103. https://doi.org/10.1097/MPA.0b013e318160748f

McPhee, I., Gibson, L.C.D., Kewney, J., Darroch, C., Stevens, P.A., Spinks, D., Cooreman, A., MacKenzie, S.J., 2005. Cyclic nucleotide signalling: a molecular approach to drug discovery for Alzheimer's disease. Biochem. Soc. Trans. 33, 3.

Metrich, M., Berthouze, M., Morel, E., Crozatier, B., Gomez, A.M., Lezoualc'h, F., 2010. Role of the cAMP-binding protein Epac in cardiovascular physiology and pathophysiology. Pflüg. Arch. Eur. J. Physiol. 459, 535–546.

Middeldorp, C.M., Vink, J.M., Hettema, J.M., de Geus, E.J.C., Kendler, K.S., Willemsen, G., Neale, M.C., Boomsma, D.I., Chen, X., 2010. An association between Epac-1 gene variants and anxiety and depression in two independent samples. Am. J. Med. Genet. B Neuropsychiatr. Genet. 153B, 214–219. https://doi.org/10.1002/ajmg.b.30976

Mohsen, K., Azzazy, H.M.E., Allam, N.K., Basalious, Emad.B., 2020. Intranasal lipid nanocapsules for systemic delivery of nimodipine into the brain: In vitro optimization and in vivo pharmacokinetic study. Mater. Sci. Eng. C 116, 111236. https://doi.org/10.1016/j.msec.2020.111236

Ohvo-Rekilä, H., Ramstedt, B., Leppimäki, P., Peter Slotte, J., 2002. Cholesterol interactions with phospholipids in membranes. Prog. Lipid Res. 41, 66–97. https://doi.org/10.1016/S0163-7827(01)00020-0

Peltier, S., Oger, J.-M., Lagarce, F., Couet, W., Benoît, J.-P., 2006. Enhanced Oral Paclitaxel Bioavailability After Administration of Paclitaxel-Loaded Lipid Nanocapsules. Pharm. Res. 23, 1243–1250. https://doi.org/10.1007/s11095-006-0022-2

Perrier, T., Saulnier, P., Fouchet, F., Lautram, N., Benoît, J.-P., 2010. Post-insertion into Lipid NanoCapsules (LNCs): From experimental aspects to mechanisms. Int. J. Pharm. 396, 204–209. https://doi.org/10.1016/j.ijpharm.2010.06.019

Prajapati, R., Fujita, T., Suita, K., Nakamura, T., Cai, W., Hidaka, Y., Umemura, M., Yokoyama, U., Knollmann, B.C., Okumura, S., Ishikawa, Y., 2019. Usefulness of Exchanged Protein Directly Activated by cAMP (Epac)1-Inhibiting Therapy for Prevention of Atrial and Ventricular Arrhythmias in Mice. Circ. J. 83, 295–303. https://doi.org/10.1253/circj.CJ-18-0743

Ramadan, A., Lagarce, F., Tessier-Marteau, A., Thomas, O., Legras, P., Macchi, L., Saulnier, P., Benoit, J.P., 2011. Oral fondaparinux: use of lipid nanocapsules as nanocarriers and in vivo pharmacokinetic study. Int. J. Nanomedicine 6, 2941–2951. https://doi.org/10.2147/IJN.S25791

Resnier, P., Galopin, N., Sibiril, Y., Clavreul, A., Cayon, J., Briganti, A., Legras, P., Vessières, A., Montier, T., Jaouen, G., Benoit, J.-P., Passirani, C., 2017. Efficient ferrocifen anticancer drug and Bcl-2 gene therapy using lipid nanocapsules on human melanoma xenograft in mouse. Pharmacol. Res., Pharmacological modulation of tumor microenvironment 126, 54–65. https://doi.org/10.1016/j.phrs.2017.01.031

Robichaux, W.G., Cheng, X., 2018. Intracellular cAMP Sensor EPAC: Physiology, Pathophysiology, and Therapeutics Development. Physiol. Rev. 98, 919–1053. https://doi.org/10.1152/physrev.00025.2017

Sasso, M.S., Lollo, G., Pitorre, M., Solito, S., Pinton, L., Valpione, S., Bastiat, G., Mandruzzato, S., Bronte, V., Marigo, I., Benoit, J.-P., 2016. Low dose gemcitabine-loaded lipid nanocapsules target monocytic myeloid-derived suppressor cells and potentiate cancer immunotherapy. Biomaterials 96, 47–62. https://doi.org/10.1016/j.biomaterials.2016.04.010

Sun, D.-P., Fang, C.-L., Chen, H.-K., Wen, K.-S., Hseu, Y.-C., Hung, S.-T., Uen, Y.-H., Lin, K.-Y., 2017. EPAC1 overexpression is a prognostic marker and its inhibition shows promising therapeutic potential for gastric cancer. Oncol. Rep. 37, 1953–1960. https://doi.org/10.3892/or.2017.5442

Takenaga, N., Hasegawa, T., Ishii, M., Ishizaki, H., Hata, S., Kamei, T., 1998. In vitro metabolism of a new anticancer agent, 6-N-formylamino-12,13-dihydro-1,11-dihydroxy-13-(β-D-glucopyranosil)5H-indolo [2,3-A]pyrrolo [3,4-C]carbazole-5,7(6H)-dione (NB-506), in mice, rats, dogs, and humans. Drug Metab. Dispos. 27, 213–220.

Thackaberry, E.A., Wang, X., Schweiger, M., Messick, K., Valle, N., Dean, B., Sambrone, A., Bowman, T., Xie, M., 2014. Solvent-based formulations for intravenous mouse pharmacokinetic studies: tolerability and recommended solvent dose limits. Xenobiotica 44, 235–241. https://doi.org/10.3109/00498254.2013.845706

Thompson, M., 1992. NTP Technical Report on toxicity studies of formic acid (CAS 64-18-6) administered by inhalation to F344/N rats and B6C3F1 mice. Toxic. Rep. Ser.

Toussaint, B., Hillaireau, H., Jaccoulet, E., Cailleau, C., Legrand, P., Ambroise, Y., Fattal, E., 2021. Interspecies comparison of plasma metabolism and sample stabilization for quantitative bioanalyses: Application to (R)-CE3F4 in preclinical development, including metabolite identification by high-resolution mass spectrometry. J. Chromatogr. B 1183, 122943. https://doi.org/10.1016/j.jchromb.2021.122943

Uster, P.S., Allen, T.M., Daniel, B.E., Mendez, C.J., Newman, M.S., Zhu, G.Z., 1996. Insertion of poly(ethylene glycol) derivatized phospholipid into pre-formed liposomes results in prolonged in vivo circulation time. FEBS Lett. 386, 243–246. https://doi.org/10.1016/0014-5793(96)00452-8

World Health Organization, 2020. World health statistics 2020: monitoring health for the SDGs, sustainable development goals. Geneva: WHO.

Zhang, M., Zheng, J., Wang, W., Kong, F., Wu, X., Jiang, J., Pan, J., 2019. Exchange-protein activated by cAMP (EPAC) regulates L-type calcium channel in atrial fibrillation of heart failure model. Eur. Rev. Med. Pharmacol. Sci. 23, 2200–2207.

Supplementary for Toussaint et al. "Stability, pharmacokinetics, and biodistribution in mice of the EPAC1 inhibitor (R)-CE3F4 entrapped in liposomes and lipid nanocapsules"

Supplementary tables

Table S1. Proportions of (*R*)-CE3F4 and lipids used for CE3F4 encapsulation in TPGS-liposomes.

TPGS-liposomes formulations		$TPGS_{Low}$	$TPGS_{Medium}$	$TPGS_{High}$	$TPGS_{Medium}$-$Chol_{Low}$	$TPGS_{Medium}$-$Chol_{Medium}$	$TPGS_{Medium}$-$Chol_{High}$
[(*R*)-CE3F4] (mM)		2.85	2.85	2.85	2.85	2.85	2.85
[Lipids] concentration (mM)		25.0	25.0	25.0	25.0	25.0	25.0
(*R*)-CE3F4/lipid ratio (mol/mol)		11.4%	11.4%	11.4%	11.4%	11.4%	11.4%
Lipid molar proportion ($n/n_{total\ lipids}$)	EggPC	79.7%	64.7%	49.7%	49.7%	39.7%	29.7%
	Cholesterol	-	-	-	15.0%	25.0%	35.0%
	DSPE-PEG_{2000}	5.3%	5.3%	5.3%	5.3%	5.3%	5.3%
	TPGS	15.0%	30.0%	45.0%	30.0%	30.0%	30.0%

Table S2. Proportions of (*R*)-CE3F4 and lipids used for CE3F4 encapsulation in DOBA-liposomes.

DOBA-liposomes formulations		$DOBA_{Low}$	$DOBA_{Medium}$	$DOBA_{High}$	$DOBA_{Medium}$-$Chol_{Low}$	$DOBA_{Medium}$-$Chol_{Medium}$	$DOBA_{Medium}$-$Chol_{High}$
[(*R*)-CE3F4] (mM)		2.85	2.85	2.85	2.85	2.85	2.85
[Lipids] concentration (mM)		25.0	25.0	25.0	25.0	25.0	25.0
(*R*)-CE3F4/lipid ratio (mol/mol)		11.4%	11.4%	11.4%	11.4%	11.4%	11.4%
Lipid molar proportion ($n/n_{total\ lipids}$)	EggPC	79.7%	64.7%	49.7%	49.7%	39.7%	29.7%
	Cholesterol	-	-	-	15.0%	25.0%	35.0%
	DSPE-PEG_{2000}	5.3%	5.3%	5.3%	5.3%	5.3%	5.3%
	DOBA	15.0%	30.0%	45.0%	30.0%	30.0%	30.0%

Table S3. Properties of surfactants used for liposomes or lipid nanocapsules formulations.

Formulation	Surfactant	EggPC	HSPC	DSPE-PEG_{2000}	PEG-HS
	Molecular mass (g/mol)	770	784	2805	960 [3]
Liposomes (bilayer)	Mean area per surfactant molecule in bilayer (nm^2)	0.61 (POPC) [1]	0.46 [1]	0.38 [2]	-
	Membrane thickness (nm)	3.43 (POPC) [1]	4.29 [1]	4.50 [2]	-
	Polymer thickness (nm)	-	-	3.80* [2]	Unknown
LNC (monolayer)	Area per surfactant molecule in monolayer (nm^2)	0.65 (POPC) [1]	-	-	0.43 [3]

*: Polymer thickness for a DSPE-PEG_{2000} proportion of 5% (mol/mol)

(1) (Drabik et al., 2020); (2): (Watkins et al., 2011); (3): (Lacoeuille et al., 2007)

Table S4. Results on EE%, and (*R*)-CE3F4's apparent half-life in murine plasma for TPGS-liposomes.

TPGS-liposomes formulations	$TPGS_{Low}$	$TPGS_{Medium}$	$TPGS_{High}$	$TPGS_{Medium}$-$Chol_{Low}$	$TPGS_{Medium}$-$Chol_{Medium}$	$TPGS_{Medium}$-$Chol_{High}$
EE (%)	99.6	97.6	102.4	101.3	92.4	36.6
(*R*)-CE3F4's apparent $t_{1/2}$ in murine plasma (h)	0.70	0.74	0.77	0.73	0.73	0.85

Table S5. Results on EE%, and (*R*)-CE3F4's apparent half-life in murine plasma for DOBA-liposomes.

DOBA-liposomes formulations	$DOBA_{Low}$	$DOBA_{Medium}$	$DOBA_{High}$	$DOBA_{Medium}$-$Chol_{Low}$	$DOBA_{Medium}$-$Chol_{Medium}$	$DOBA_{Medium}$-$Chol_{High}$
EE (%)	86.9	84.5	57.4	88.8	32.3	23.7
(*R*)-CE3F4's apparent $t_{1/2}$ in murine plasma (h)	0.74	0.71	0.72	0.71	0.75	0.72

Table S6. Detailed steps and calculated parameters used to estimate the potential (*R*)-CE3F4 surface density and the number of (*R*)-CE3F4 molecules per liposome (EggPC, HSPC) or lipid nanocapsule (LNC_1, LNC_1-$CE3F4_{High}$).

Step	Parameter	Liposomes		Lipid nanocapsules	
		EggPC	HSPC	LNC_1	LNC_1-$CE3F4_{High}$
Calculation of the virtual surfactant surface	EggPC (molecules/mL)	1.26×10^{19}	-	7.12×10^{18}	7.12×10^{18}
	HSPC (molecules/mL)	-	1.10×10^{19}	-	-
	$DSPE\text{-}PEG_{2000}$ (molecules/mL)	7.05×10^{17}	6.14×10^{17}	-	-
	PEG-HS (molecules/mL)	-	-	3.19×10^{19}	3.19×10^{19}
	Total surface's tensioactives calculated (nm^2/mL)	7.95×10^{18}	5.28×10^{18}	1.83×10^{19}	1.83×10^{19}
Estimation of the total surface of one particle	D_H measured (nm)	90.0	106	29.3	29.6
	Outer surface (nm^2/particle)	21331	30419	2697	2753
	Inner surface (nm^2/particle)	17927	25345	-	-
	Total particle's surfaces (nm^2/particle)	39258	55764	2697	2753
Estimation of the number CE3F4 molecules per particle	CE3F4 (molecules/mL)	1.46×10^{18}	1.20×10^{18}	1.56×10^{18}	2.99×10^{18}
	Number of particles/mL	2.03×10^{14}	9.47×10^{13}	6.81×10^{15}	6.66×10^{15}
	Surface density of CE3F4 (CE3F4/nm^2 of lipids)	0.18	0.23	0.09	0.16
	Number of CE3F4/particle	7187	12680	229	449

Supplementary figures

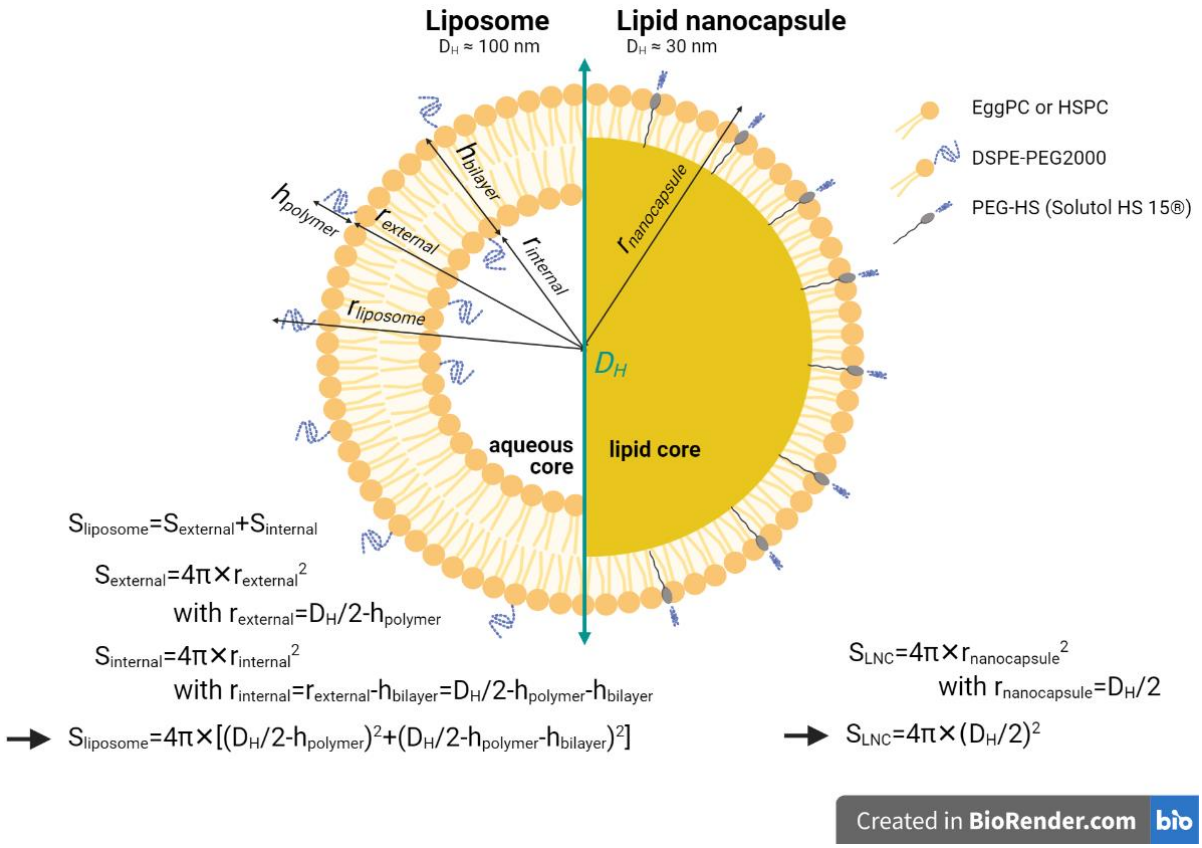

Figure S1. Structural organization of a liposome (left) and a lipid nanocapsule (right), and related surface's calculations. D_H: hydrodynamic diameter.

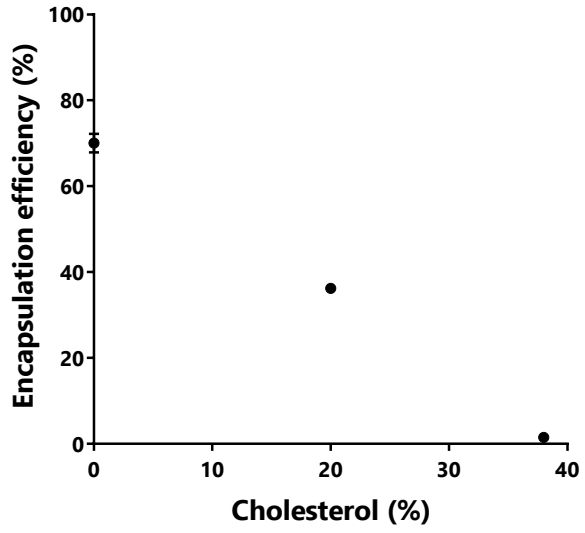

Figure S2. Influence of the cholesterol proportion on (*R*)-CE3F4 encapsulation efficiency for liposomes made with HSPC.

References for the Supporting Information

Drabik, D., Chodaczek, G., Kraszewski, S., Langner, M., 2020. Mechanical Properties Determination of DMPC, DPPC, DSPC, and HSPC Solid-Ordered Bilayers. Langmuir 36, 3826–3835. https://doi.org/10.1021/acs.langmuir.0c00475

Lacoeuille, F., Hindre, F., Moal, F., Roux, J., Passirani, C., Couturier, O., Cales, P., Le Jeune, J.J., Lamprecht, A., Benoit, J.P., 2007. In vivo evaluation of lipid nanocapsules as a promising colloidal carrier for paclitaxel. International Journal of Pharmaceutics 344, 143–149. https://doi.org/10.1016/j.ijpharm.2007.06.014

Watkins, E.B., El-khouri, R.J., Miller, C.E., Seaby, B.G., Majewski, J., Marques, C.M., Kuhl, T.L., 2011. Structure and Thermodynamics of Lipid Bilayers on Polyethylene Glycol Cushions: Fact and Fiction of PEG Cushioned Membranes. Langmuir 27, 13618–13628. https://doi.org/10.1021/la200622e